AGU PUBLICATIONS

JGR

Journal of Geophysical Research: Atmospheres

RESEARCH ARTICLE
10.1002/2015JD024637

Key Points:
- Boundary layer injections favor new particle formation
- A multistep growth process of freshly formed particles is suggested
- Possible nucleation criteria and important factors controlling nucleation rates are assessed

Supporting Information:
- Supporting Information S1
- Figure S1
- Figure S2
- Figure S3
- Figure S4
- Figure S5
- Figure S6

Correspondence to:
J. Tröstl and M. Gysel,
jasmin.troestl@gmx.at;
martin.gysel@psi.ch

Citation:
Tröstl, J., et al. (2016), Contribution of new particle formation to the total aerosol concentration at the high-altitude site Jungfraujoch (3580 m asl, Switzerland), *J. Geophys. Res. Atmos.*, *121*, 11,692–11,711, doi:10.1002/2015JD024637.

Received 11 DEC 2015
Accepted 17 JUN 2016
Accepted article online 8 SEP 2016
Published online 6 OCT 2016

Contribution of new particle formation to the total aerosol concentration at the high-altitude site Jungfraujoch (3580 m asl, Switzerland)

Jasmin Tröstl[1], Erik Herrmann[1], Carla Frege[1], Federico Bianchi[1,2], Ugo Molteni[1], Nicolas Bukowiecki[1], Christopher R. Hoyle[1,3], Martin Steinbacher[4], Ernest Weingartner[1,5], Josef Dommen[1], Martin Gysel[1], and Urs Baltensperger[1]

[1]Laboratory of Atmospheric Chemistry, Paul Scherrer Institute, Villigen, Switzerland, [2]Department of Physics, University of Helsinki, Helsinki, Finland, [3]WSL Institute for Snow and Avalanche Research SLF, Davos, Switzerland, [4]Empa, Swiss Federal Laboratories for Materials Science and Technology, Dübendorf, Switzerland, [5]Now at Institute of Aerosol and Sensor Technology, School of Engineering, University of Applied Sciences, Windisch, Switzerland

Abstract Previous modeling studies hypothesized that a large fraction of cloud condensation nuclei (CCN) is attributed to new particle formation (NPF) in the free troposphere. Despite the potential importance of this process, only few long-term observations have been performed to date. Here we present the results of a 12 month campaign of NPF observations at the high-altitude site Jungfraujoch (JFJ, 3580 m above sea level (asl)). Our results show that NPF significantly adds to the total aerosol concentration at the JFJ and only occurs via previous precursor entrainment from the planetary boundary layer (PBL). Freshly nucleated particles do not directly grow to CCN size (90 nm) within observable time scales (maximum 48 h). The contribution of NPF to the CCN concentration is low within this time frame compared to other sources, such as PBL entrainment of larger particles. A multistep growth mechanism is proposed which allows previously formed Aitken mode particles to add to the CCN concentration. A parametrization is derived to explain formation rates at the JFJ, showing that precursor concentration, PBL influence, and global radiation are the key factors controlling new particle formation at the site.

1. Introduction

According to recent modeling studies, up to 45% of cloud condensation nuclei (CCN) are secondary aerosol particles formed in the atmosphere via new particle formation (NPF), with a large fraction formed in the free troposphere (FT) [*Merikanto et al.*, 2009]. In the planetary boundary layer (PBL), new particle formation events have been frequently observed and continuously monitored at many sites around the world including observations in boreal forests [*Kulmala et al.*, 2013], urban [e.g., *Xiao et al.*, 2015; *Betha et al.*, 2013], rural and coastal areas [*Liu et al.*, 2008]. Monitoring new particle formation events at high altitudes over a long period is, however, technically challenging. The Jungfraujoch (JFJ) is a high-altitude site in the Swiss Alps and is in the FT for a substantial fraction of the time (especially in winter). Compared to other high-altitude stations, it is easy to access, making it a unique site for atmospheric observations.

The Global Atmosphere Watch (GAW) program includes several stations at high altitude, where NPF has been observed, e.g., Storm Peak Laboratory (USA), Pyramid Station (Nepal), JFJ's Sphinx Laboratory (Switzerland), and Chacaltaya (Bolivia). *Venzac et al.* [2008] conducted a 16 month campaign at the Pyramid station at 5079 m above sea level (asl). An average event frequency (percentage of days on which NPF was observed) of 45% was found at this location. *Hallar et al.* [2011] showed frequent observations (52% of the days) of new particle formation at Storm Peak observatory during several periods between 2001 and 2009. A distinct seasonality was observed at Storm Peak, with the maximum nucleation event frequency in spring and the minimum in summer [*Yu and Hallar*, 2014; *Hallar et al.*, 2016]. *Boulon et al.* [2010] investigated nucleation and growth of ultrafine charged aerosols at the JFJ, finding an event frequency of about 17%. *Rose et al.* [2015a] observed one of the highest nucleation event frequencies of about 64%, and in the dry season up to 100% at Chacaltaya (5240 m asl) in Bolivia.

Although NPF in the FT could potentially account for a large fraction of atmospheric particles [*Merikanto et al.*, 2009], our knowledge of aerosol nucleation at high altitude is limited particularly with respect to the

precursor species. Models have shown that nucleation events at Storm Peak in spring are most likely associated with sulfuric acid, whereby NPF events in summer could have been driven by low-volatility organics [*Yu and Hallar*, 2014]. To date, even the most advanced global aerosol models include FT nucleation only via a single pathway (binary sulfuric acid-water nucleation) [*Carslaw et al.*, 2013].

Recently, *Herrmann et al.* [2015] reported the aerosol number size distribution at the JFJ over a 6 year period, also considering the role of NPF. However, for this study only the aerosol size distribution above a diameter of 20 nm and formation rates of aerosol particles with a diameter of 10 nm were available. *Bianchi et al.* [2016] investigated the chemical composition of the nucleating molecular clusters for the first time at the JFJ, showing that highly oxygenated molecules (HOMs) or sulfuric acid together with ammonia are required to explain the observed formation rates, with HOMs driving NPF during most events. These data were collected during the NUcleation, CLoud, and Aerosol Characterization Experiment (NUCLACE) campaign which included two intensive observation periods (IOP1: 7 January to 3 March 2013; IOP2: 13 January to 5 March 2014) during which several state-of-the-art instruments to investigate NPF were installed at the JFJ, and a long-term observation period (LOP) extending from 23 July 2013 to 11 June 2014 with a smaller set of instruments including a nano-scanning mobility particle sizer (nano-SMPS), a low cutoff condensation particle counter (CPC), and an atmospheric pressure interface time-of-flight mass spectrometer (APi-TOF).

This work focuses on the physical properties rather than on the detailed chemistry of NPF events. We use the nano-SMPS and the low cutoff CPC data from the NUCLACE LOP data set to further assess the contribution of nucleation events to the total particle and the cloud condensation nuclei (CCN) number concentrations at the JFJ and investigate the role of PBL influence on new particle formation. We also show to what extent the formation rates observed at the JFJ are driven by possible controlling factors such as organic vapors, solar radiation, PBL influence, and aging. A parametrization to derive nucleation rates is discussed.

2. Methods

2.1. Site Description and Instrumentation

The Sphinx laboratory of the high-alpine research station JFJ (3580 m asl; 46.55°N, 7.98°E) is located on a crest between the summits of two mountains, the Jungfrau (4158 m asl) in the southwest and the Mönch (4089 m asl) in the northeast (Figure 1a). Therefore, local wind observations show mainly northwesterly or southeasterly direction. The distribution of wind directions during the LOP can be found in Figure 1b. Due to its remote location, the JFJ is considered to be a continental background site [*Nyeki et al.*, 1998].

The JFJ is classified as a global station in the Global Atmosphere Watch (GAW) program and is part of the Swiss National Air Pollution Monitoring Network (NABEL). The laboratory is equipped with a large number of instruments for monitoring aerosol properties as well as greenhouse and reactive gases [*Bukowiecki et al.*, 2016]. Trace gas observations used in this study are carbon monoxide (CO) measurements made with Cavity Ring-Down Spectrometry [*Zellweger et al.*, 2012] and the sum of oxidized nitrogen species (NO_y) measured after conversion of NO_y to NO by chemiluminescence [*Pandey Deolal et al.*, 2012]. In addition, meteorological parameters such as temperature, pressure, global radiation, wind speed and direction, and relative humidity are monitored by MeteoSwiss. In winter, the JFJ has been found to be in the FT most of the time; however, a significant PBL influence is observed (up to 80% of the time in summer and as low as 30% in winter) [*Herrmann et al.*, 2015].

For this work, the nano-SMPS and SMPS (both custom-built TSI-type [*Wang and Flagan*, 1990]) are used to derive the size distribution from 5 to 600 nm. The total aerosol concentration above a diameter of 10 nm is measured with a CPC 3772 and the concentration above a diameter of 3.2 nm with a CPC 3776 (both TSI). Aerosol size information throughout the text is given in mobility diameter, all times are UTC + 1, i.e., local time without daylight saving time in summer.

As we consider particles with diameters below 50 nm, the aerosol concentration is corrected for diffusion losses in the sampling lines. To keep the diffusion losses and thus the corrections small, the nano-SMPS and the CPC 3776 were installed with two individual sampling lines of only 65 cm length each. Additionally, core sampling probes were installed [*Wimmer et al.*, 2015]. The core sampling probe uses a makeup flow of 5 L min^{-1} to increase the flow in this 65 cm sampling line. Right before the instruments, the actual sample aerosol flow of 1 L min^{-1} is extracted from the middle of the tubing using an isokinetic probe. In that way, we could decrease the residence time in the sampling line to one sixth of its original value. The diffusion losses were

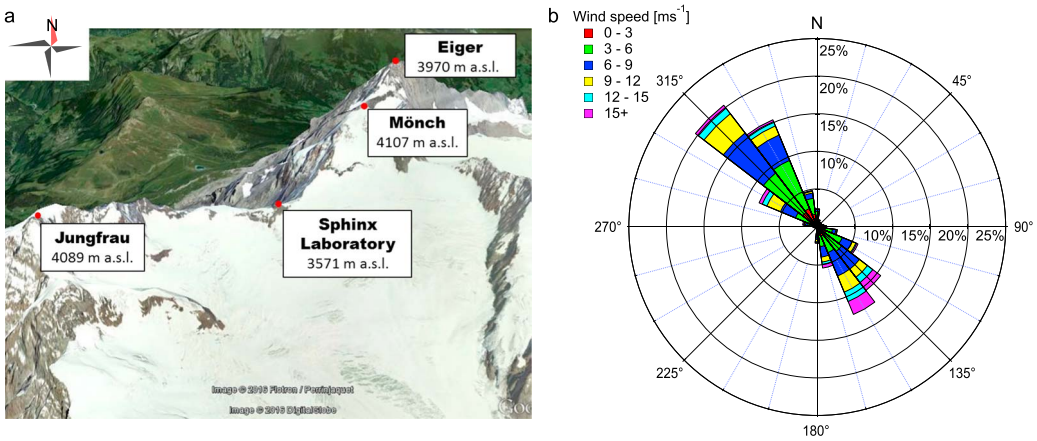

Figure 1. (a) Satellite view of the JFJ and surroundings (map data: ©Google Earth 2015, DigitalGlobe 2015). (b) Wind direction and speed during NUCLACE.

calculated for laminar flow conditions [*Kulkarni et al.*, 2011] and determined to be less than 10% for 5 nm particles and around 15% for 3 nm particles. The nano-SMPS data were additionally corrected for diffusion losses in the neutralizer (Krypton-85) and the differential mobility analyzer column (DMA) assuming an effective length of 1 and 7.1 m, respectively [*Wiedensohler et al.*, 2012]. The major part of the sampling line was outside the building and heated slightly above 0° to avoid clogging by frozen water. The rest of the sampling line and the instruments were at room temperature. The SMPS and the CPC 3772 were installed at the total aerosol inlet of the Sphinx [*Weingartner et al.*, 1999]. Setup and SMPS data analysis were described in detail by *Jurányi et al.* [2011].

The SMPS and nano-SMPS agree within 10% for the overlapping size range 20–90 nm when corrected for diffusion losses, charging efficiency, and CPC detection efficiency (Figure S1 in the supporting information (SI)). Comparison between CPC 3772 and CPC 3776 at times when the cutoff difference is of minor influence indicates a reproducibility of the particle number concentration measurements of approximately ±20% (Figures S2 and S3).

Signals from pollution due to local activities were removed from the data set upon visual inspection of single size distributions. Local pollution can be identified by its short-lived and drastic fluctuations in the aerosol properties [*Herrmann et al.*, 2015]. Sources of local pollution include helicopter engines, diesel generators, and construction work as well as smoking on the visitor terrace of the Sphinx laboratory [*Fröhlich et al.*, 2015].

2.2. NPF Event Classification

Days during NUCLACE were classified upon visual inspection of the contour plot of the nano-SMPS aerosol number size distribution. Additionally, the appearance times of clusters measured with the APi-TOF were compared with the appearance time of 3.2 nm particles to differentiate between true NPF events and transport processes. We differentiate between in-situ, off-site, none, and unclassified event days. In-situ NPF events comprise events when either nucleation or growth or both were observed in-situ. This requires either stagnant conditions or a homogeneous distribution over a large area. The events were split into three groups, 1A, 1B, and 2 based on previous work [*Hirsikko et al.*, 2007; *Boulon et al.*, 2010]. An additional class of "off-site" NPF events was introduced to describe the observation of nucleation and Aitken mode particles (<10 nm and <50 nm, repetitively) arriving at the JFJ, without any direct evidence of nucleation and growth. These were not included in the NPF event statistics. The characteristic features in the observations at the JFJ of each event type are as follows:

1. In-situ events
    a. Type 1A
        Clear nucleation event with appearance of freshly nucleated particles (increase in the concentration of the CPC 3776 and the lowest size bins of the nano-SMPS) and subsequent, continuous growth to larger particles over several hours, finally reaching 10 nm in diameter or more. The shape of the

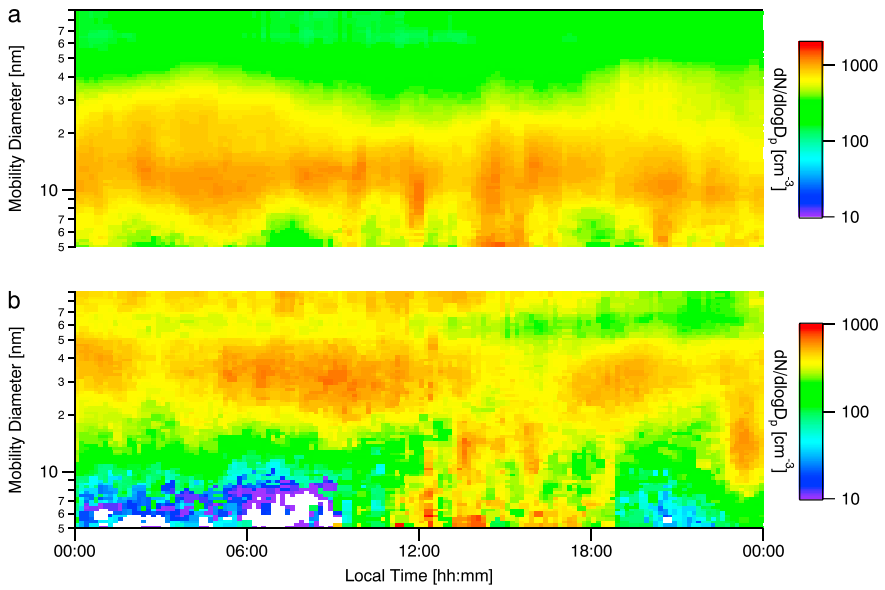

Figure 2. Average image plot of (a) Aitken band off-site events and (b) nucleation mode events, excluding days with simultaneous in-situ events.

growing mode in the aerosol number size distribution is very distinct (high number concentration and clearly visible, continuous growth). In this category we also included particularly strong events with high formation rates and very fast growth in the beginning which were interrupted by an air mass change shortly after the onset of nucleation, if the modal size became larger than 10 nm before interruption.

b. Type 1B

These are also clear nucleation events exhibiting the key features described for type 1A, however, with a less distinct shape of the event, i.e., lower concentration in the growing particle mode and interruptions of the growth at an early stage (<10 nm). Here we do not differentiate between several type 1B subclasses, as their identification would require an aerosol size distribution below 5 nm.

c. Type 2

Nucleation is clearly occurring at the Jungfraujoch; however, the shape of the growing mode is not well defined or noncontinuous growth is observed, making it difficult to analyze the formation rate and growth rate. Thus, at least one parameter (formation rate or growth rate) could not be determined.

2. Off-site events

a. Aitken mode bands

A distinct and very narrow mode of small particles in the size range 10–50 nm is frequently observed at the JFJ. Furthermore, the modal size and number concentration of particles of the mode typically remain stable over time. These stable bands were sometimes observed over several days indicating a highly homogeneous distribution over a large area. They can also appear under conditions when nucleation is normally not expected to occur, e.g., at nighttime or when the JFJ is below clouds. An average daily image plot of the aerosol number size distribution of all Aitken mode off-site events, excluding days with in-situ events is displayed in Figure 2a. The key features of in-situ NPF (nucleation and growth) are not observed. The sources of these bands are most likely NPF events that occurred off-site, but their growth stopped before arrival at the JFJ. A primary aerosol source is considered to be very unlikely, as it would have different characteristics, i.e., broader mode and larger sizes. Also, the concentration would likely be more variable in time, as there are no primary sources at these altitudes which are homogeneously distributed over large areas. It is thus very likely that these off-site nucleation events have occurred within the lower FT similar to the type 1A or 1B events and were subsequently spatially distributed and further diluted, eventually reaching the JFJ.

b. Nucleation mode particles during vertical uplifting

During sunny conditions vertical uplifting is frequently observed at the JFJ. At the same time nucleation mode particles (<10 nm) can often be observed, without any further growth. These particles

could be a result of a supersaturation of condensable vapors during this vertical uplifting, yielding a locally limited burst of new particles that is then observed at the JFJ. These nucleation mode particles can sometimes be observed during the night, but not very frequently. The major difference between the Aitken mode bands and the nucleation mode particles is the duration of such events. The nucleation mode particles are a rather short-lived phenomenon (can be as short as 1 h) and indicate a local phenomenon which just passes through the JFJ, whereas the Aitken mode bands are very stable and long lasting (up to several days) indicating a homogeneous distribution over a large area. This is also visible in Figure 2b, which displays an average daily image plot of the aerosol number size distribution of nucleation mode off-site events. In contrast to the Aitken band, nucleation mode particles only appeared during a short time and mostly during the day, when vertical transport is expected. Similar off-site events have been observed in the marine boundary layer, where the increase in the concentration of small particles was associated with convective air [*Rose et al.*, 2015b]. A similar phenomenon with reverse direction has been observed by *O'Dowd et al.* [2010], where nucleated particles where entrained from the FT to the marine boundary layer. Further, *Yu and Hallar* [2014] observed short-lasting bursts of ultrafine particles in summer, which were associated with off-site nucleation events in sulfuric acid plumes.

3. Non-events
   No typical features of in-situ or off-site nucleation events (see above) were observed. Non-event days often occur under cloudy conditions, whereas in-situ nucleation events always occur under sunny conditions or after cloud evaporation. Therefore, we define a subclass of sunny nonevent days based on the global radiation data. Contrasting these non-event days with in-situ event days aims at identification of factors that favor or suppress nucleation other than cloudiness.
4. Unclassified
   Days when it was not possible to determine the event type. This could be due to noisy data (low counting statistics), an increase in the local pollution obscuring a possible nucleation event, or data gaps.

2.3. Formation and Growth Rate Determination

2.3.1. Formation Rates

The formation (or nucleation) rate J_D corresponds to the number of particles crossing a certain diameter D per time unit and per unit volume. It is typically expressed in $cm^{-3}\ s^{-1}$. Assuming a concentration $N_{D_{min}-D_{max}}$ (in cm^{-3}) in a certain size range from D_{min} to D_{max}, a change in this concentration during a nucleation event at the JFJ can result from the following sink and source terms: (1) particles growing into the detection range, which corresponds to the true formation rate $J_{D_{min}}$; (2) particles growing out of the detection range (R_{growth}); (3) particle coagulation (R_{coag}); (4) net transport of particles at the JFJ including dilution ($R_{NetTrans}$); and (5) local primary sources ($R_{primary}$). Thus, $dN_{D_{min}-D_{max}}/dt$ represents an apparent formation rate that consists of the following terms [*Bianchi et al.*, 2016]:

$$\frac{dN_{D_{min}-D_{max}}}{dt} = J_{D_{min}} - R_{growth} - R_{coag} + R_{NetTrans} + R_{primary} \quad (1)$$

As a basis for the calculation we used the CPC 3776 concentration $N_{3.2-1000}$. Due to the high cutoff of the CPC, it is very unlikely that aerosol particles grow out of the CPC upper detection limit, so that R_{growth} is virtually zero. During nucleation events, meteorological conditions at the JFJ were typically stable. The background aerosol concentrations were rather low, such that nucleation events typically cause a substantial increase of the total particle number concentration. This implies that the contribution of the background aerosol to the term $R_{NetTrans}$ during air mass changes (e.g., after change of wind direction) and during vertical transport (e.g., appearance of particles below 10 nm) is typically negligible. Still, transport processes could influence the determined nucleation rates, but an exact quantification is not possible which increases the uncertainty of the determined formation rates. We further assume that NPF events are spatially homogeneously distributed over a large area, as is commonly done. With this approach, we neglect $R_{NetTrans}$ in the calculation of J_D but consider it in the uncertainty estimation of the formation rate (see SI and below). Changes due to local sources such as cigarette smoke were identified and removed, as previously stated; thus, $R_{primary}$ does not need to be considered. Therefore, only coagulation losses over the full size range need to be corrected for. The coagulation sink, S_{coag} (s^{-1}), for a particle with a certain diameter D_j is determined in the following way [*Kulmala et al.*, 2012]:

$$S_{coag}(D_j) = \sum_{D_i'=D_j}^{D_{max}} K(D_i', D_j) N_{D_i'} \quad (2)$$

where $K(D_j, D_i')$ is the coagulation coefficient ($cm^3\ s^{-1}$) between two particles with diameters D_j and D_i' corrected for the transition regime using the Fuchs correction factor [*Seinfeld and Pandis*, 2006]. $N_{D_i'}$ is the number concentration (cm^{-3}) in a certain size range with D_i' being the diameter midpoint of this size bin (geometric mean of size bin boundaries). For the calculation of S_{coag}, the concentration of the combined nano-SMPS and SMPS aerosol size distribution from 10 to 600 nm was used. Below 10 nm, the nano-SMPS size distribution was not used due to high uncertainties in the diffusion loss correction of the nano-SMPS system and in the charging equilibrium. Thus, one additional size bin from 3.2 to 10 nm was inserted, which was derived from the difference $N_{3.2-1000} - N_{10-1000}$ (CPC 3776 − CPC 3772). From 3.2 nm to 10 nm the coagulation rate decreases exponentially, so that using the diameter midpoint could be misleading. Therefore, 3.2 nm was chosen as the representative diameter for this lowest size bin, such that the calculation provides an upper limit of S_{coag}. The coagulation correction term was then determined in the following way [*Kürten et al.*, 2015]:

$$R_{coag}(D_{min}) = \frac{1}{2} \sum_{D_j=D_{min}}^{D_{max}} \sum_{D_i'=D_{min}}^{D_{max}} \cdot K(D_i', D_j) \cdot N_{D_i'} \cdot N_{D_j} \quad (3)$$

with the factor 1/2 avoiding double counting of collisions due to the double summation [*Seinfeld and Pandis*, 2006]. The summation was done over all size bins j of the combined size distribution. $J_{3.2}$ is then calculated as follows:

$$J_{3.2} = \frac{dN_{3.2-1000}}{dt} + R_{coag}(3.2) \quad (4)$$

In the end, $J_{3.2}$ and $dN_{3.2}/dt$ were often within 5%, and thus, a correction would not have been needed for most events. However, all stated $J_{3.2}$ values do include a coagulation correction.

The CPC concentration accuracy is 20%, the coagulation correction adds an additional uncertainty of 5%, as we only estimate an upper limit. Uncertainties related to transport have been estimated to 25% (Figure S4). Formation rate uncertainties were determined to be 50% in total.

2.3.2. Growth Rates

The growth rate (GR) is defined as the change of the diameter per time unit, dD/dt, and is typically expressed in nm h^{-1}. A Gaussian least square fit is applied to the temporal evolution of the concentration of a nano-SMPS size bin. Due to noise in the data especially in the lowest size bins, the Gaussian fit is needed to capture the correct peak and shape of the change in concentration. The Gaussian fit is also only applied to a certain time range of the event, where the concentration is increasing. The decrease in concentration is not included in the fit. The background aerosol concentration was used to constrain the baseline of the fit and was held constant. The 50% rise time (t_{50}) is defined as the time at half rise of the fitted Gaussian. For each nano-SMPS size bin, we calculated the corresponding t_{50}. The growth rates were calculated from the slope of a linear least square fit through the diameter versus rise time data in the size range 5–15 nm and 15–30 nm.

An alternative method to obtain growth rates would be to follow the mode, median, or geometric mean diameter of the number size distribution [*Kulmala et al.*, 2012]. However, at low sizes these diameters might not be determined correctly due to a possible bias in the uncertainties of the diffusion correction and charging equilibrium. The determination of the rise time is independent of these uncertainties.

Growth rate determination methods in general have mainly two sources of uncertainties [*Yli-Juuti et al.*, 2011]. If the nucleation event is spatially heterogeneously distributed, the growth rate may appear faster or more slowly than it actually is for an individual particle. Also, several peaks can be observed in the concentration time series making it difficult to decide which peak should be followed. These methods are therefore prone to subjective errors.

3. Results and Discussion

3.1. Event Statistics and Meteorology

Figure 3 shows the frequency of all event types during NUCLACE. An average event frequency of approximately 17–20% was observed for types 1A, 1B, and 2 events, which is comparable to an earlier study at the JFJ by *Boulon et al.* [2010]. During the NUCLACE campaign, the JFJ was in or below clouds approximately 50% of the time. This reduces global radiation and thus limits the photochemistry necessary to form low-volatility vapors, such as sulfuric acid and highly oxygenated molecules (HOMs). Additionally, in-cloud conditions

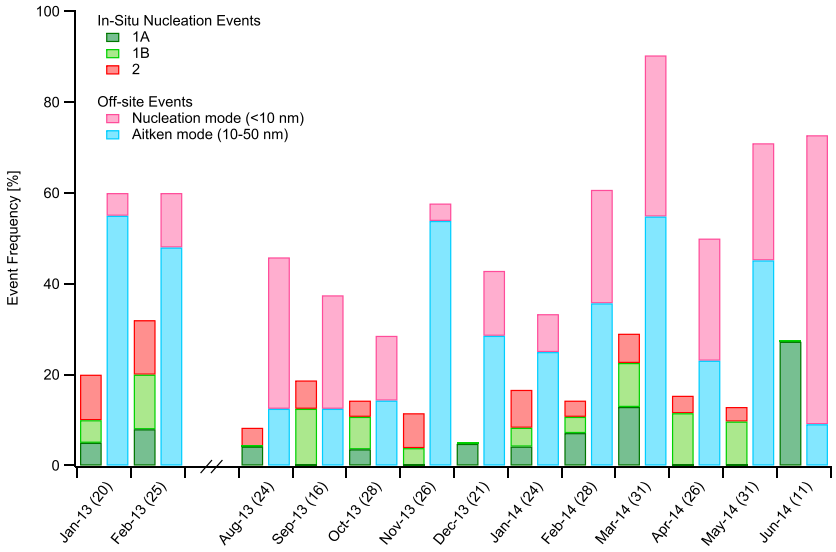

Figure 3. Nucleation event frequency in monthly bins during NUCLACE 2013/2014 (IOP1, IOP2, and LOP). In-situ nucleation events were observed on approximately 18% of the campaign days. Off-site events were more frequent with an event frequency of approximately 55%. Available days per month are indicated in the brackets. In total, the in-situ and off-site events can be >100%, as in-situ and off-site events can be observed during the same day.

increase the condensation sink prohibiting aerosol nucleation. The actual NPF frequency during sunny days is ~40%. Off-site nucleation events were detected during approximately 55% of the days, whereby Aitken mode bands were also observed during below-cloud days, when in-situ nucleation events were not. In-situ and off-site events add up to >100% for some months, because they occasionally took place during the same day.

No clear seasonality was found for in-situ nucleation events. A clear seasonal pattern is observed for the off-site events. Nucleation mode events are mostly observed during warmer seasons (spring through fall), when vertical transport occurs more frequently. During these periods, vertical transport is likely to occur. Aitken mode events were mostly observed during colder periods, when stable conditions were present (winter and spring).

The formation rates $J_{3.2}$ varied between 0.2 and 7.5 cm^{-3} s^{-1} with a mean formation rate of 1.8 cm^{-3} s^{-1} for type 1A events and 0.7 cm^{-3} s^{-1} for type 1B events. The growth rates varied between 1.6 and 10 nm h^{-1} for type 1A events and between 0.9 and 11.9 nm h^{-1} for type 1B events. The mean growth rates for the nucleated particles in the size range between 5 and 15 nm were 4 nm h^{-1} for type 1A and 4.8 nm h^{-1} for type 1B events. Both, nucleation and growth rates, are comparable to other FT sites, as summarized by *García et al.* [2014]. Further details can be found in Table 1.

In the following, meteorological properties of type 1 events are compared to those of sunny non-event days and the full LOP in order to determine meteorological factors that possibly favor nucleation. In summer, off-site nucleation events are very common, due to the favored vertical transport. Thus, no sunny non-event day was found during this season. As a consequence, the category "sunny non-event" could show a seasonal bias in the meteorological data. Therefore, we additionally show the category "sunny" for reference, which includes all days with a global radiation ≥90% of the daily, expected maximal global radiation in the category sunny. In a next step, we determined the average monthly values of each meteorological parameter for an equal representation to minimize the seasonal bias. In Figure 4, variability of temperature, relative humidity, absolute water content, and global radiation are shown as box plots. The typical time window for nucleation to occur is between 09:00 and 15:00. Therefore, the median (horizontal line), the 25th and 75th percentiles (boxes), and the 10th and 90th percentiles (whiskers) of sunny non-event days, all sunny days (monthly average), and all campaign days were calculated for this time window. For nucleation days, these values were taken during the time when nucleation and growth were observed, to get statistics of the conditions during NPF.

The temperatures during sunny non-events are slightly higher compared to type 1 events, all sunny days, and the campaign average, despite the exclusion of the summer months. A strong effect of the temperature, however, was not observed, although one might expect an influence of the temperature as observed in laboratory studies [*Kirkby et al.*, 2011].

Table 1. Overview of Observed Nucleation and Growth Rates During the NUCLACE Measurement Campaign

Type 1A				Type 1B			
Date	$J_{3.2}$ (cm^{-3} s^{-1})	GR 5–15 nm ($nm\ h^{-1}$)	GR >15 nm ($nm\ h^{-1}$)	Date	$J_{3.2}$ (cm^{-3} s^{-1})	GR 5–15 nm ($nm\ h^{-1}$)	GR >15 nm ($nm\ h^{-1}$)
24/01/2013	0.3	4.5	-	16/01/2013	0.5	2.4	2.6
08/02/2013	0.8	3.2	6	09/02/2013	0.4	7.9	-
26/02/2013	0.3	2	1.5	22/02/2013	0.6	2.2	-
25/08/2013	-	2.7	2.3	24/02/2013	0.2	3.3	-
12/10/2013[a]	-	8.8	3.5	02/09/2013[a]	-	8.8	-
21/12/2013[a]	-	3.3	3	24/09/2013[a]	-	2.5	5.6
24/01/2014	0.8	2.8	-	06/10/2013[a]	-	6.4	-
11/02/2014	1.4	2.1	-	24/10/2013[a]	-	5.2	4.3
27/02/2014	7.5	10	7.9	23/11/2013[a]	-	11.9	-
02/03/2014	4.8	4.8	-	21/01/2014	1.2	4.5	-
05/03/2014	1.5	3.8	-	15/02/2014	0.2	1.4	-
20/03/2014	1.1	3.9	-	06/03/2014	-	2.6	-
28/03/2014	1.1	1.6	-	18/03/2014	0.6	2.9	5.5
05/06/2014	-	4.4	-	25/03/2014	0.9	0.9	3
07/06/2014	1.0	2.3	-	01/04/2014	-	6	-
08/06/2014	0.9	4.1	6.5	06/04/2014	1.5	5.8	-
				10/04/2014	-	8.2	-
				06/05/2014	-	2.3	-
				24/05/2014	1.4	3.3	-
				28/05/2014	-	6.9	-
Mean	1.8	4.0	4.4	Mean	0.7	4.8	4.2
Median	1.0	3.6	3.5	Median	0.6	3.9	4.3
STD	2.1	2.3	3.5	STD	0.4	2.9	4.3

[a]CPC 3776 not available.

The global radiation is decreased for sunny non-event days compared to all sunny days, which is due to the seasonal bias of sunny non-events. Type 1 events show a slightly higher value compared to the campaign average. This is expected, as photochemistry is essential for the formation of low-volatility vapors, such as sulfuric acid and HOMs.

The relative humidity (RH) is considerably lower on sunny non-event days and sunny days compared to type 1 events and the campaign average, while the absolute water content is lower on sunny non-event days only. An increased nucleation probability in air masses with high RH is possibly related to increased abundance of condensable vapors through the following causalities [*Kulmala et al.*, 2014]. First, the increased RH could be an indicator of PBL influence, which increases the concentration of precursor gases. Sunny conditions without recent PBL contact are often characterized by low RH (typical FT conditions). Second, a lower water content also leads to a lower OH radical concentration, which could lower the production of low-volatility vapors.

Figure 5 shows the average wind direction for nucleation events and sunny non-events. During nucleation events, the wind direction was mainly from southeast. Non-event days behave similar to the campaign average, with the wind coming mostly from the northwest (for campaign average see Figure 1). As mentioned previously, the approaching air masses are funneled by the surrounding mountains thus confining observed local wind directions to either northwest or southeast. Therefore, the wind direction alone cannot be used as indicator for the exact air mass origin. *Bianchi et al.* [2016] further investigated the origin of the air masses in detail using the Lagrangian particle dispersion model FLEXPART [*Stohl et al.*, 2005] for the same nucleation and sunny non-events as presented here. The most pronounced ground contact before arrival at the JFJ occurred at middistance including regions in northern France and also southern Italy when averaged over all air masses of type 1A events. Type 1B events also showed the most pronounced ground contact at larger

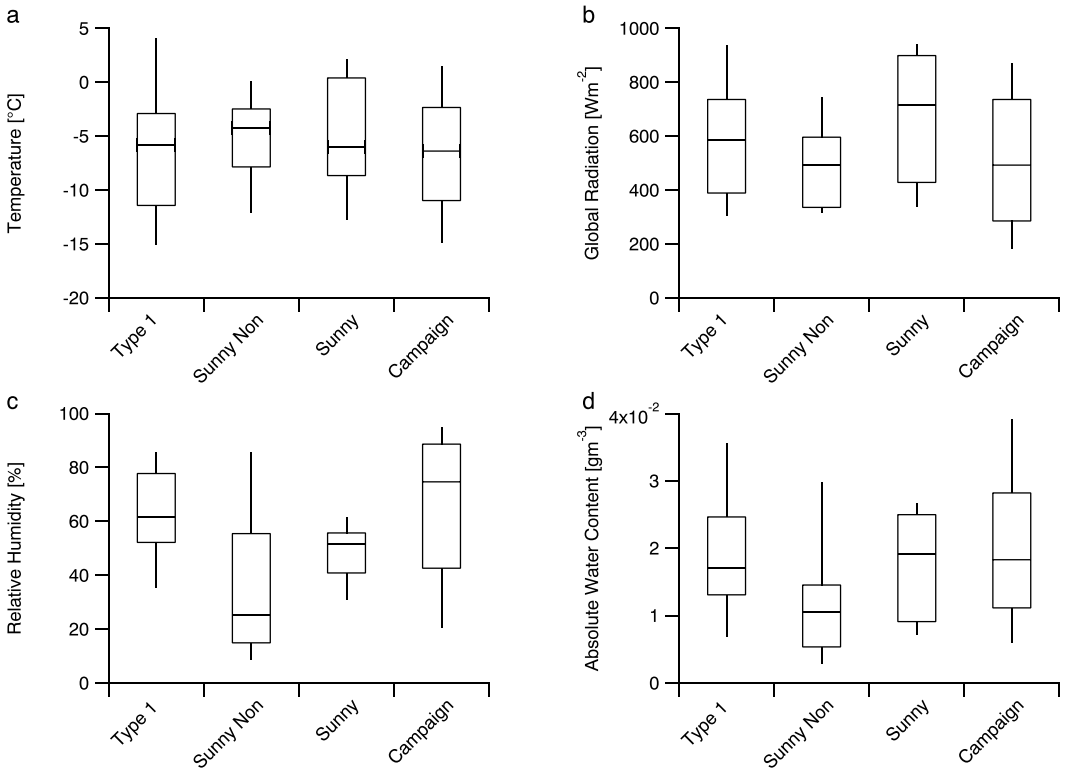

Figure 4. (a) Temperature, (b) global radiation, (c) relative humidity, and (d) absolute water content of type 1, sunny non-events, all sunny days, and all campaign days. Median (horizontal line), the 25th and 75th percentiles (boxes), and the 10th and 90th percentiles (whiskers) of sunny non-event days, all sunny days, and all campaign days were calculated between 09:00 and 15:00. For the type 1 nucleation days, values during the time, when NPF was observed, were used.

distance including northern France, northern Germany, and the Benelux. Sunny non-events on the other hand showed generally small ground contact at larger distances.

3.2. Factors Controlling Nucleation at the JFJ

A previous study indicated that NPF at the JFJ is linked to PBL influence [*Bianchi et al.*, 2016]. During a large fraction of the year (especially in winter), the JFJ is considered to be in the lower free troposphere

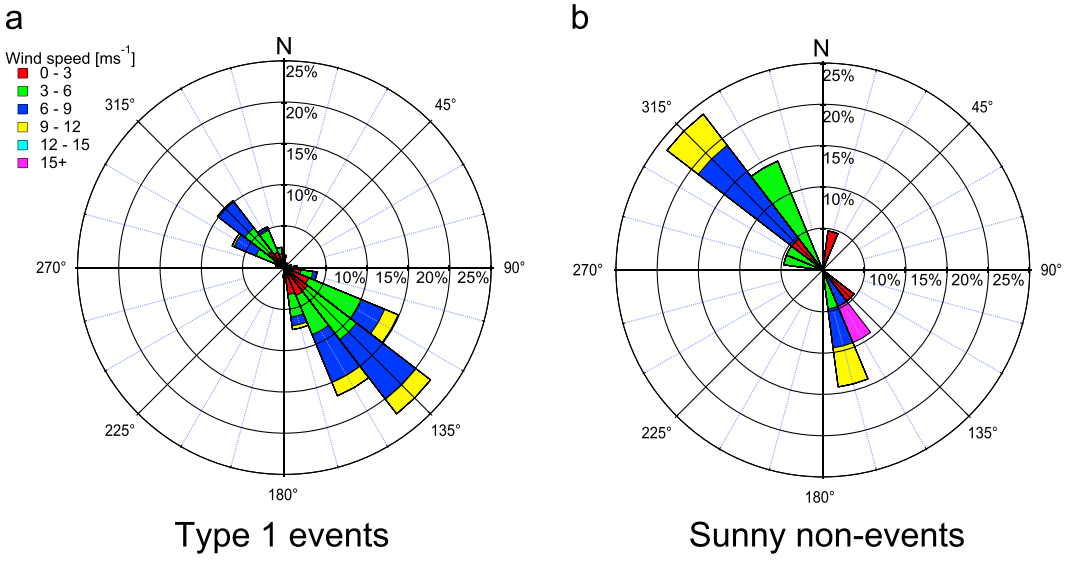

Figure 5. Wind directions and speeds of (a) type 1 events and (b) sunny non-event days.

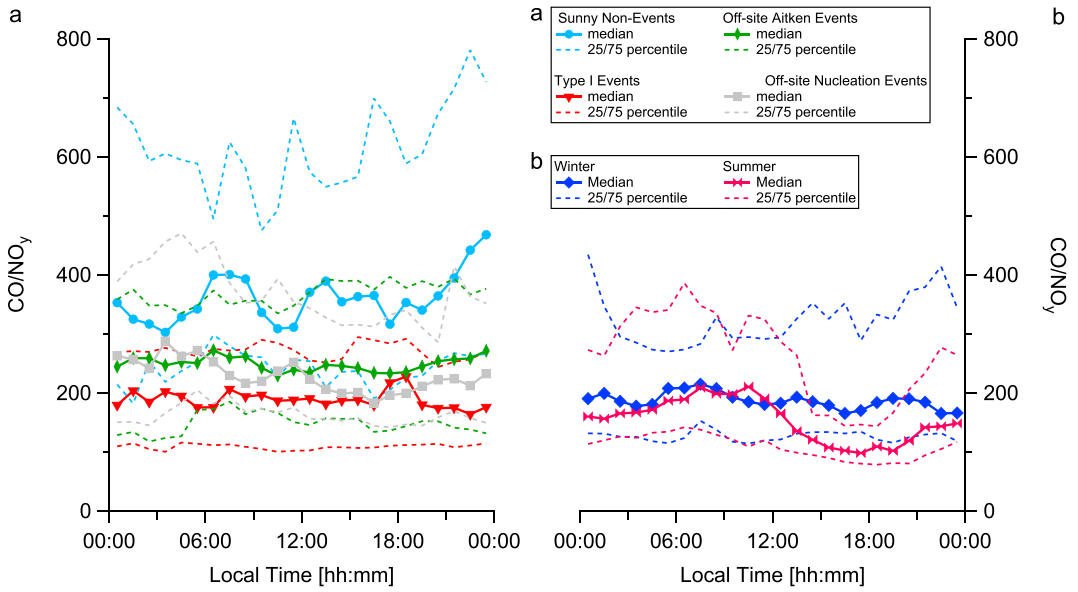

Figure 6. (a) Diurnal variation of CO/NO_y for type 1, off-site Aitken and nucleation events, and sunny non-event days of the LOP. (b) Diurnal variation of CO/NO_y during winter (December 2013, January 2014, and February 2014) and summer (August 2013 and June 2014) days of the LOP, where in summer a PBL influence due to vertical transport is expected. Ratios above 100 indicate air masses from anthropogenic sources after transport or dilution, which is typically the case for air masses arriving at the JFJ. Ratios between 200 and 500 indicate FT conditions.

[*Collaud Coen et al.*, 2011; *Herrmann et al.*, 2015]. The JFJ is very rarely in the PBL, but PBL influence is observed throughout the year and is most pronounced in summer. Mountain ranges favor the transport of PBL air toward the FT, creating the so-called injection layer [*Nyeki et al.*, 2000; *Henne et al.*, 2005a; *Nyeki et al.*, 2002]. This injection layer is decoupled from the PBL and comprises about 20–30% air that originated in the PBL [*Henne et al.*, 2005b]. In summer, the JFJ can sit within this injection layer, which can reach up to 4000 m asl [*Nyeki et al.*, 2000]. Aerosol particle, precursor and oxidant concentrations are elevated in the injection layer compared to clean FT air masses [*Henne et al.*, 2005a].

The CO/NO_y ratio was found to be a proxy for the age of an air mass [*Zellweger et al.*, 2003]. At the JFJ, the CO/NO_y ratio can be used to estimate the time since (and strength of) the last PBL contact of the air mass. Ratios of 6.25–10 are observed close to anthropogenic sources. Ratios >100 indicate either a strong contact with subsequent long-range transport and dilution or a weak, recent contact. For free tropospheric conditions, values between 200 and 500 are observed at the JFJ depending on the seasonality (500 in winter, 200 in summer). As a remote site, JFJ is characterized by values above 100, whereby lower values (down to 20) can be observed during strong PBL influence. After a PBL injection, CO/NO_y continuously increases with time, approaching clean FT conditions [*Herrmann et al.*, 2015].

Figure 6 shows the median diurnal variation of CO/NO_y for (a) type 1, off-site, and sunny non-event days and (b) winter 2013/2014 and summer 2013 days. Sunny non-event days are characterized by a high ratio, indicating rather clean free tropospheric conditions (corresponding to $N_{90} < 60\ cm^{-3}$ according to *Herrmann et al.* [2015]). For the type 1 events, this ratio is lower and around 200 indicating a very recent weak PBL influence or a strong PBL influence several days before arrival at the JFJ. This is in agreement with *Bianchi et al.* [2016] who showed that nucleation at the JFJ is favored within a short time period (24–48 h) after the last PBL contact of the air mass, as determined with FLEXPART dispersion modeling. If the observed nucleation mode particles were due to transport of PBL air into the FT directly at the JFJ, the CO/NO_y ratio would be seen to reduce rapidly during the arrival of this air mass. As CO/NO_y ratios were rather constant throughout the nucleation event days, this scenario can be ruled out. This conclusion is further supported by Figure 6b. For winter months, the JFJ is expected to be most of the time in the free troposphere [*Herrmann et al.*, 2015]. As a result, vertical transport is hardly observed and therefore CO/NO_y ratios do not show a diurnal pattern.

During summer, CO/NO_y started decreasing around noon and only increased again after sunset, reflecting the time window when the injection layer can expand up to 4000 m asl [*Nyeki et al.*, 2000]. From the 25th

Table 2. Summary of Variables and Fit Parameters Used to Parametrize $J_{3.2}$[a]

Parametrization of $J_{3.2}$	a	b	c	d	e	f	g	h	χ^2
$a \cdot [CO]^b$	$2.32 \cdot 10^{-7}$	3.13	-	-	-	-	-	-	1.75
$a \cdot [Rad]^c$	$3.02 \cdot 10^{-3}$	-	0.88	-	-	-	-	-	1.81
$a \cdot [S_{coag}]^d$	42.8	-	-	0.43	-	-	-	-	1.96
$a \cdot [CO/NO_y]^e$	3.4	-	-	-	−0.27	-	-	-	2.55
$a \cdot [NO_y]^f$	0.9	-	-	-	-	0.4	-	-	2.31
$a \cdot [RH]^g$	1.75	-	-	-	-	-	−0.18	-	2.71
$a \cdot [T]^h$	1.81	-	-	-	-	-	-	−0.12	3.37
$a \cdot [CO]^b \cdot [Rad]^c$	$1.56 \cdot 10^{-6}$	2.02	0.54	-	-	-	-	-	1.44
$a \cdot [CO]^b \cdot [S_{coag}]^d$	$3.7 \cdot 10^{-4}$	2.02	-	0.21	-	-	-	-	1.61
$a \cdot [CO]^b \cdot [Rad]^c \cdot [S_{coag}]^d$	$2.7 \cdot 10^{-6}$	1.98	0.51	0.019	-	-	-	-	1.44
$a \cdot [CO]^b \cdot [S_{coag}]^d \cdot [CO/NO_y]^e$	$5.7 \cdot 10^{-3}$	1.57	-	0.25	−0.05	-	-	-	1.62
$a \cdot [CO]^b \cdot [Rad]^c \cdot [CO/NO_y]^e$	$5.5 \cdot 10^{-5}$	1.38	0.63	-	−0.19	-	-	-	1.37

[a]The used variables were CO (ppb), global radiation (Rad) (W m^{-2}), coagulation sink (S_{coag}) (s^{-1}), NO_y (ppb), relative humidity (RH) (%), and temperature (T) (K). χ^2 is used as measure for the goodness of fit.

and 75th percentiles it is visible that the CO/NO_y in the morning varies strongly in summer. For days with very low values, the decrease is not as dominant. This can happen when PBL air was entrained very recently (the day before), so that the air mass did not restore to FT conditions yet. Under such conditions, an additional injection only slightly decreases the ratio. When looking at the summer event days separately, they only show a slight but distinct decrease in the afternoon (thus not visible in the yearly median), so that it is difficult to differentiate if the nucleation was triggered by an injection on the same or on a previous day as suggested by *Bianchi et al.* [2016] (see Figure S5 and Supporting Information S1).

Off-site Aitken events showed higher CO/NO_y ratios than type 1 events. We hypothesize that in these cases the particle formation resulted from an injection that occurred more than two days before arrival at the JFJ. However, we cannot determine if nucleation happened in the PBL or in the FT. During off-site nucleation days, the CO/NO_y ratios were slightly elevated in the morning but decreased around noon, which is the typical onset time for vertical transport. This supports our hypothesis of local nucleation mode particle bursts during vertical uplifting.

3.3. Parametrization of Observed Formation Rates

Following the qualitative analysis of the PBL influence, we will now use additional factors such as the global radiation (Rad), temperature (T), relative humidity (RH), CO as indicator for the concentration of aerosol precursors, and condensation sink (S_{cond}), to quantitatively determine their influence on the formation rates. Only limited knowledge of the concentrations of the precursor species is available. The nucleating compounds have been identified by *Bianchi et al.* [2016] using APi-TOF measurements for the same events showing that sulfuric acid is of minor importance for nucleation at the JFJ. Furthermore, the SO_2 concentration is very low and below the detection limit most of the time (see Figure S6 in the SI). SO_2 is therefore not considered. *Bianchi et al.* [2016] showed that the identified HOMs differed from the ones found in the nucleation and initial growth of α-pinene oxidation products in the absence of sulfuric acid [*Kirkby et al.*, 2016; *Tröstl et al.*, 2016]. They therefore hypothesized that at the JFJ the nucleating HOMs originate in the PBL from anthropogenic rather than biogenic sources, even though the latter could not be excluded. Thus, we use the CO concentration as a tracer for PBL influence, which implicitly is an indicator for the organic precursors forming the HOMs.

We cannot determine the diffusion coefficient of the organic nucleating species, which is necessary to determine S_{cond}. Therefore, we use S_{coag} calculated at a fixed diameter of 3.2 nm as a proxy for S_{cond}. For such small diameters, S_{cond} and S_{coag} are highly correlated; thus, using S_{coag} implicitly considers the combined effect of precursor losses due to condensation and losses of newly formed particles due to coagulation.

We applied least square fits (minimizing χ^2) to assess the importance of several parameters and variables or combinations of them as summarized in Table 2. This parametrization could only be done on a subset of 14 NPF events, for which all variables were available.

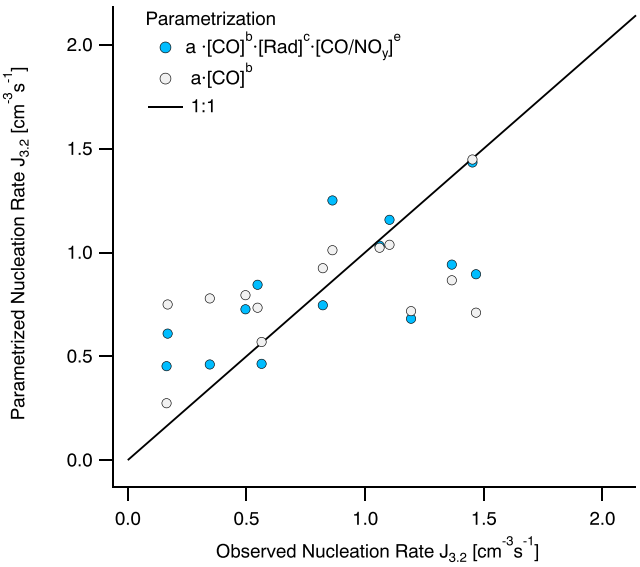

Figure 7. Comparison of observed and parametrized nucleation rates calculated with the best parametrization using global radiation, CO, and CO/NO_y (blue) and using the best single variable fit (grey).

In an initial step, we tested how well single variables correlated with the formation rate $J_{3.2}$ (see Table 2). Temperature and RH show the highest χ^2 and are not further considered at this point. Although CO, CO/NO_y, S_{coag}, and the global radiation already show a low χ^2, one variable does not satisfactorily describe the observed formation rates. By combining these best correlations, χ^2 further decreases. Additionally, we tested different combinations of three variables including CO, CO/NO_y, S_{coag}, and global radiation. Combining CO, CO/NO_y, and the global radiation yielded the best result with $\chi^2 = 1.37$. However, already a combination of CO and radiation gives a good result with $\chi^2 = 1.44$. The addition of CO/NO_y thus only causes a modest improvement of the fit. Finally, a fit involving all four variables listed above did not lead to further improvement. Moreover, the fits always yielded a positive exponent for S_{coag}, which is physically unexpected. Adding more variables such as RH and temperature does not further improve the goodness of the fit. One also has to note that while introducing more variables and fit parameters could mathematically improve the fit, the interpretation would be quite difficult due to the limited number of data points. Figure 7 shows the best fit results of the parametrization using CO, global radiation, and CO/NO_y and the best single variable fit using CO.

From Table 2 it is not directly obvious to which factors the formation rate is most sensitive, as the used input variables have different units and magnitudes, so that the magnitude of the derived fit parameters does not directly show the importance of the input variable. Therefore, we used the best fit parametrization to perform a sensitivity analysis. For this we used the interquartile ranges and the median of the variables CO, CO/NO_y, and the global radiation. We compared the resulting formation rate using the median values to the values obtained by exchanging one median value either with the 25th percentile or the 75th percentile of one variable only, leaving the median values of the others fixed. Using the 25th/75th percentiles, the formation rate changed by +11.8%/−4.1% for CO, −7.8%/+6.6% for CO/NO_y and +22.4%/−15.8% for global radiation. The formation rate is thus most sensitive to global radiation and the CO concentration which directly corresponds to the available concentration of condensable vapors. The PBL influence as determined by the CO/NO_y ratio has the weakest impact of these three variables on the formation rates, probably because the effect is already mostly covered by CO.

Due to the small subset of observations and the lack of precursor quantification, this parametrization cannot provide a complete representation of the factors controlling nucleation at the JFJ. Nevertheless, it gives some further insight into nucleation criteria at the JFJ. Meteorological parameters such as temperatures and RH seem to have a minor impact on the formation rate at the JFJ in contrast to our expectations. A temperature dependence of formation rates has been observed previously in the laboratory [*Kirkby et al.*, 2011]. This dependence could be obscured by other factors more important for nucleation at the JFJ. The RH was significantly higher on in-situ event days compared to sunny non-event days. The poor correlation of RH with the

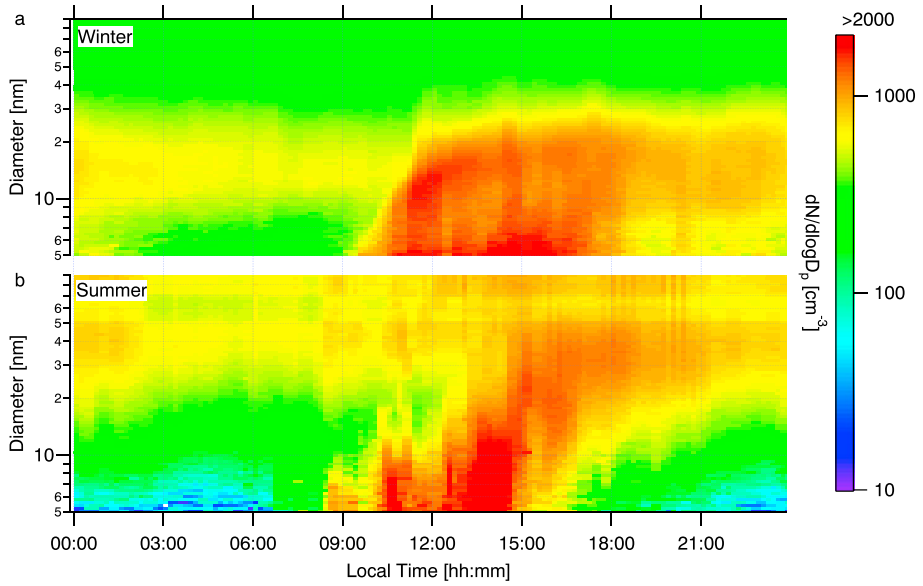

Figure 8. Average, diurnal (UTC + 1 h) size distribution from 5 to 80 nm as seen by the nano-SMPS. Average (a) over winter days and (b) over summer days. For the winter period, 104 days from December 2013, January 2014, February 2014, and March 2014 were used (including all available data). In the summer period, 82 days from May 2014, June 2014, August 2013, and September 2013 were averaged (again all available data). May 2014 and September 2013 were additionally included as not many days during the meteorological summer were available.

formation rate suggests that the elevated RH on in-situ event days mostly reflects the recent PBL influence. Further, the positive correlation with S_{coag} indicates that the coagulation/condensation sink is not a limiting factor for NPF at the JFJ due to the generally low values. S_{coag} and S_{cond} are even higher on events days compared to non-event days, as also reported by *Boulon et al.* [2010], so that this positive correlation is attributable to condensing vapors due to PBL injections. The variables used for our best estimate are indicators for the PBL influence (CO/NO_y), the required photochemistry (global radiation), and the proxy of aerosol precursor concentration (CO). In summary, the availability of condensable vapors and global radiation is more important than the condensation sink and meteorological parameters at the JFJ.

3.4. Particle Production Due To NPF

Figure 8 shows the seasonal diurnal pattern of the mean total aerosol number size distribution from 5 to 80 nm (all days). Figure 8a shows winter months and Figure 8b summer months during NUCLACE LOP. We compare these two seasons as the difference in the PBL influence is most prominent. Confirming findings from the previous section, the growth stops at ~30 nm in winter, with a mode diameter of ~20 nm, due to the shorter daytime (less radiation) and less available vapors (less photochemistry and/or less PBL influence). Nucleating particles can be observed until 18:00. A persistent band is visible around 10–30 nm. This band most likely originates from previous nucleation events, either at the JFJ or off-site. Growth stops as well around 18:00 and the concentration of nucleated particles decreases. This is most likely due to air exchange in the free troposphere, allowing undisturbed air masses to reach the JFJ.

For the summer months (Figure 8b), the particles reach ~50 nm, with a mode diameter of ~30 nm. This is most likely due to the longer sunshine duration and the higher intensity in summer which allows for more photochemistry and thus stronger oxidation of the aerosol precursors and also more time to grow the freshly nucleated particles. Nucleating particles can only be observed until 15:00, which is earlier than in winter. The stronger PBL influence in summer results in an enhancement of the aerosol precursor concentrations; however, the higher condensation sink (and possibly a higher temperature) could counteract nucleation at an earlier stage than in winter, whereby it was shown in the previous section that the condensation sink in general is not a limiting factor at the JFJ. A persistent band in the Aitken mode is observed similar to winter; however, with a mode diameter at ~40 nm. This band likely originates from two processes. On the one hand NPF in the FT is followed by transport to the JFJ. On the other hand, a large contribution to the aerosol number size distribution from convective uplifting is observed. During day time, the concentration of this band,

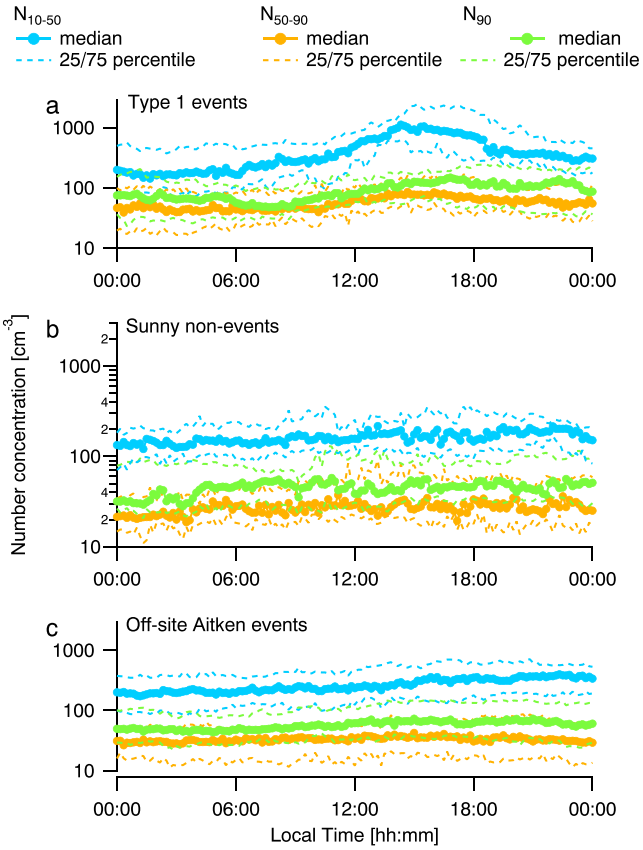

Figure 9. Diurnal variation of $N_{10–50}$, $N_{50–90}$, and N_{90} for (a) type 1 events, (b) sunny non-events, and (c) off-site Aitken mode events. Symbols represent median values, dashed lines the 25th and 75th percentiles.

and also the concentration of larger sizes, increases, which is not observed in winter, as also reported by *Herrmann et al.* [2015]. We also see the appearance of particles <10 nm without growth due to off-site nucleation events. Growth of newly formed particles is mostly observed in the afternoon, whereby NPF events were sometimes observed before noon. Thus, there is a distinct difference between winter and summer NPF.

In Figure 9, we further investigate the direct impact of NPF on the particle number concentration in three different size ranges: (1) 10–50 nm ($N_{10–50}$), (2) 50–90 nm ($N_{50–90}$), and (3) >90 nm (N_{90}). The figure shows the median diurnal variation of the number concentration for these three size ranges for (a) type 1 events, (b) sunny non-events, and (c) off-site Aitken mode events. First, we consider the particle number concentration in the 10–50 nm size range, as the nucleated particles do not grow directly beyond this size during in-situ nucleation (as seen in Figure 8). During NPF events, the number concentration $N_{10–50}$ increases by an order of magnitude from 100 particles to over 1000 particles cm^{-3} during the typical time window (09:00–15:00) when NPF was observed. This number is very likely to come solely from the NPF events. This is supported by the flat CO/NO_y ratio shown in Figure 6, indicating that vertical transport during these events yielding additional particles was of minor importance. The later decrease around 18:00 in $N_{10–50}$ is explained by air exchange, allowing undisturbed air masses to reach the JFJ as discussed above, or potentially scavenging in clouds. During off-site nucleation events, $N_{10–50}$ is slightly increased compared to sunny non-event days and lower compared to type 1 nucleation days. This supports our hypothesis that these particles nucleated elsewhere and got diluted during the transit time between the location of the nucleation event and the JFJ.

At the JFJ, the mean CCN activation diameter is typically at about 90 nm [*Jurányi et al.*, 2011; *Hammer et al.*, 2014]. The nucleated particles did not reach this diameter within the accessible time frame of 1 day. Nucleation at the Jungfraujoch therefore does not directly contribute to the CCN number concentration (see Figure 8), while growth of preexisting particles due to condensation across the CCN size threshold will be addressed below.

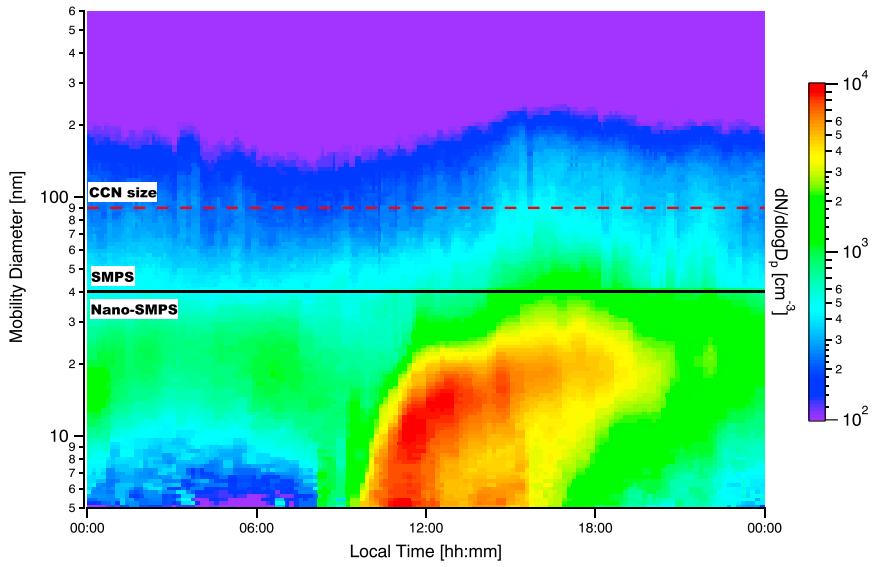

Figure 10. Diurnal pattern of average aerosol number size distribution of type 1 nucleation events. Nucleated particles do not directly grow to CCN size. However, during NPF, preexisting aerosol particles grow into the CCN size range. The red dashed line indicates the CCN threshold at the JFJ (that is a diameter of at least 90 nm). The black solid line marks the range of the used instruments (nano-SMPS below 40 nm, SMPS above 40 nm).

The coagulation sink for particles >10 nm is typically below 10^{-6} s^{-1} outside clouds as determined from the SMPS, resulting in a lifetime of several days, making in-cloud scavenging the likeliest sink. Thus, under cloud-free conditions, these particles can further grow during the following days, suggesting that a multistep growth process allows for particles nucleated at the JFJ to reach CCN size.

Next, we consider particles in the size range 50–90 nm and above 90 nm. During type 1 events, the number of particles with diameters between 50 and 90 nm and larger than 90 nm increases during the typical time window for nucleation events. This is due to the condensation of vapors on preexisting particles growing them into these size ranges. This is supported by Figure 10, which combines SMPS and nano-SMPS data for type 1 nucleation days when both instruments collected data (21 out of 36 event days without data gaps during the event days for both instruments). Preexisting particles grow simultaneously with NPF and reach diameters above 90 nm. Approximately 50–100 cm^{-3} particles (median) grew above 90 nm during NPF events. In principle, this is to be regarded as an upper limit, as part of these particles could originate from the PBL. However, this number is likely to be very close to the true number, as no decrease in the CO/NO_y ratio was observed on these days indicating stable conditions. The change of N_{90} during nucleation events can thus likely be explained by the growth of preexisting particles in the Aitken mode.

To consider a possible multistep growth of nucleated particles, we further investigated the off-site nucleation events (see event description). These events can be observed at the JFJ during 55% of the days. Here we only consider Aitken mode events, as the growth is not fast enough to grow nucleation mode particles to diameters larger than 90 nm on the same day. Figure 11 shows four example observations, which support our proposed multistep mechanism. The Aitken mode bands can be observed over days during stable conditions and also during the night, as their lifetime can be rather long in the FT (see Figure 11c). These narrow bands appear frequently and look very similar to the bands formed in a nucleation event (see Figures 11a and 11b). However, their concentration is lower as dilution has already taken place. Event a (2 March 2014) is a particularly strong nucleation with subsequent growth over a period of 9 h. Event b (25 August 2013) was another strong nucleation event; however, the growth could not be fully observed. This interruption was caused by an air mass change evidenced by an abrupt change in wind direction. During event d (27 February 2013), a band appeared right before the nucleation event. A fraction of those particles that nucleated earlier could eventually reach CCN size via a multistep growth process in the FT. This mechanism was also observed at different high-altitude stations such as Pyramid station and Chacaltaya, as visible from the aerosol number size distribution [*Venzac et al.*, 2008; *Rose et al.*, 2015a], but it was not directly addressed. This multistep growth process could therefore be important at other high-altitude sites as well.

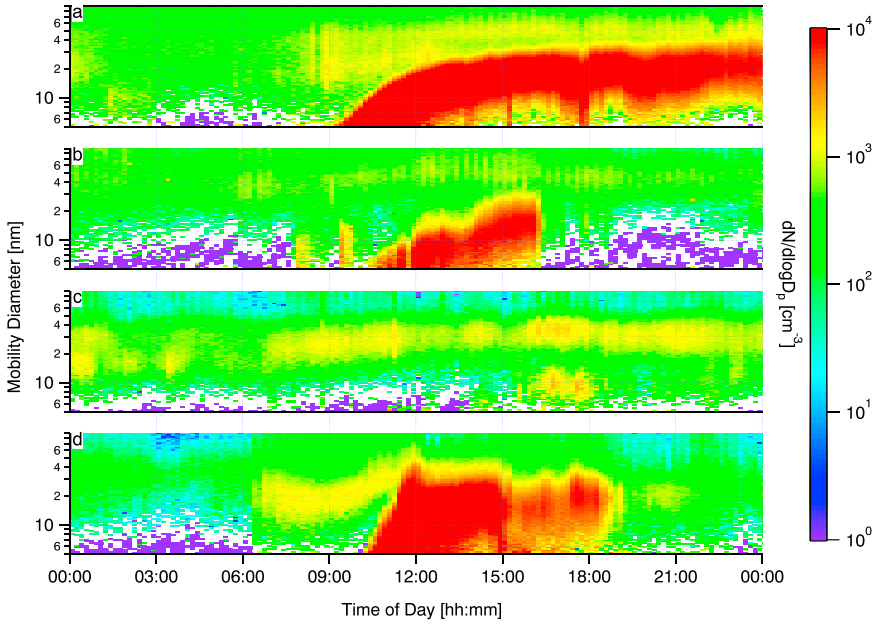

Figure 11. Comparison of four example Aitken mode particle observations. (a) Very strong nucleation with subsequent growth of several hours (2 March 2014). (b) Also a strong nucleation event; however, the growth could not be fully observed due to a change in wind direction and thus air mass change (25 August 2013). (c) Aitken mode particles appearing with only minor growth (11 March 2014). (d) Preexisting band with growth during the nucleation (17 February 2014).

To further differentiate between NPF and PBL contribution to the CCN number concentration and to confirm the findings on a longer and thus more robust data set, we consider the diurnal variation of N_{10-50}, N_{50-90}, and N_{90} for (a) winter and (b) summer, during a 6 year period in Figure 12 (the same data set that served as a basis for *Herrmann et al.* [2015]). In winter, a change in N_{10-50} is visible, with ~100 cm^{-3} additional particles in this size range appearing in the time window when NPF occurs. In comparison, Figure 9 showed that ~1000 cm^{-3} are formed during an NPF event. To compare this to Figure 12, this number (~1000 cm^{-3}) needs to be scaled with the in-situ NPF event frequency of ~20%. This yields 200 cm^{-3}, so that the change in N_{10-50} can be explained by in-situ NPF. It needs to be noted that the event frequency can vary significantly from year to year.

N_{50-90} and N_{90} slightly increase during the typical time of nucleation. As argued already above, this was most likely due to the growth of preexisting larger particles in the Aitken mode. These preexisting particles most likely resulted from NPF and indeed contributed to the CCN concentration via a multistep growth process as depicted in Figures 10 and 11d, so that NPF may be a main source of CCN in winter at the JFJ.

In summer, the background concentration N_{10-50} is very similar to winter. The increase is approximately a factor of 2 higher compared to winter (~200 cm^{-3} in summer and ~100 cm^{-3} in winter). Also, the temporal evolution looks different, showing two peaks, a short one in the morning and a longer one starting around noon. This is in agreement with Figure 8b, where the first peak is due to arriving nucleation mode particles and the second peak due to NPF events. The background concentration and the increase in N_{50-90} and N_{90} in summer is much higher compared to winter and also much higher compared to Figure 9 and can therefore not be explained by the growth of preexisting particles. The concentrations also show a double-peak feature. The first peak starts around 08:00 in the morning and the second around noon. The first increase in N_{50-90} and N_{90} is most likely due to local upslope venting caused by heating of the mountain slopes. The second peak is observed in parallel to the decrease in the CO/NO$_y$ ratio and is most likely a result of the approaching injection layer. The increase is in agreement with a previous study [*Herrmann et al.*, 2015], where it is shown that N_{90} increases by ~170 cm^{-3} (median) during PBL injections at the JFJ.

To summarize, our data indicate that in winter nucleation at the JFJ is due to the oxidation of aerosol precursors entrained from the PBL (with a window of opportunity of approximately 24–48 h ago according to *Bianchi et al.* [2016]). In summer, nucleation is also accompanied by an increase of aerosol precursor concentrations due to PBL injections. NPF can be observed before noon, when it is likely that the precursors have

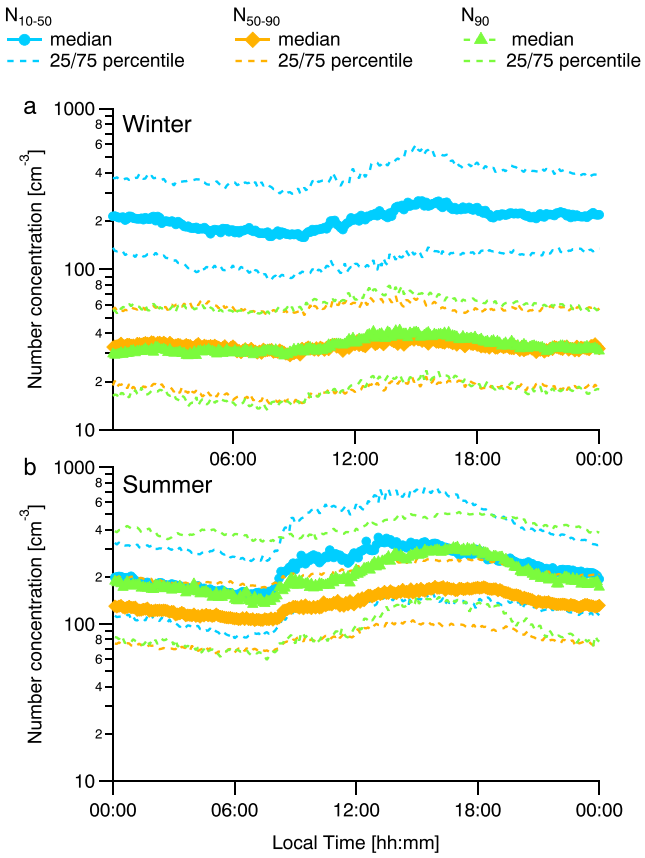

Figure 12. Diurnal variation of N_{10-50}, N_{50-90}, and N_{90} in (a) winter and (b) summer during a 6 year period (2008–2014). Symbols represent median values and dashed lines the 25th and 75th percentiles.

been entrained before, similar to winter nucleation events, or by local upslope winds. Or it can be observed in the afternoon, when the entrainment occurred via the injection layer, immediately triggering nucleation and subsequent growth to larger sizes (see also Supporting Information S1 and Figure S5). Therefore, in summer it is not possible to clearly identify if the nucleation was triggered by an injection 24–48 h ago, as is typical for winter, or by an injection at the same day, because the PBL injections occur too frequently. Also, it cannot be determined if the JFJ was actually within the injection layer or not, for this additional measurements (e.g., lidar) would be required, which was not available during NUCLACE. The major fraction of N_{90} at the JFJ is expected to be entrained from the PBL and did not form via condensation during NPF. In contrast, NPF could be a major source of CCN at the JFJ in winter, via a multistep growth process of nucleated particles.

4. Conclusions

We observed NPF at the high-altitude site JFJ during a 12 month period using a nano-SMPS and a condensation particle counter. We reported formation and growth rates and investigated the impact of NPF on the aerosol number size distribution and discussed key factors controlling NPF at the JFJ.

All nucleation events took place in perturbed FT conditions; i.e., PBL injections are essential at the JFJ to trigger nucleation. In winter, CO/NO_y ratios indicate that the PBL injections took place 24–48 h before arrival at the JFJ, confirming the window of opportunity introduced by *Bianchi et al.* [2016]. In summer, however, it is difficult to define the exact length of this window, due to the very frequent PBL injections. Summer nucleation events could thus be triggered by previously entrained precursors or by PBL injections on the same day.

The NPF frequency was determined to be approximately 20%. The JFJ was ~50% of the days in or below clouds during the LOP. Under these conditions, NPF is not observed due to the higher condensation sink and reduced photochemistry. The event frequency during sunny days is therefore ~40%. The frequency of nucleation events at the JFJ is comparable to that observed at several other high-altitude sites such as

Dome C (Antarctica) [*Järvinen et al.*, 2013], Puy de Dôme (France) [*Boulon et al.*, 2011], and Mukteshwar (India) [*Neitola et al.*, 2011], but not as high as, e.g., at Chacaltaya (Bolivia) [*Rose et al.*, 2015a]. Based on our findings, the reason for these differences is most likely the availability of nucleating species due to stronger PBL influences at other sites, as well as the weather conditions.

The impact of NPF at the JFJ is highly significant for the particle number concentration in the size range up to 50 nm. The total particles concentration can increase by up to 10,000 cm^{-3} for single events. Nucleation adds ~1000 particles cm^{-3} (median) to the aerosol concentration below 50 nm. For comparison, the average aerosol background concentration in the Aitken mode is ~500 cm^{-3} in summer and ~200 cm^{-3} in winter [*Herrmann et al.*, 2015]. The freshly nucleated particles grow up to 50 nm which is far below 90 nm, the typical activation cutoff for droplet activation around the JFJ. The nucleated and grown particles have a sufficiently large size to survive several days in the FT, so that they could grow further during the following days. Thus, a multistep growth process is necessary and possible to produce CCN size particles as a consequence of NPF (e.g., Figures 11d and 10). An average contribution to the CCN number concentration due to growth of preexisting particles of approximately 100 cm^{-3} per type 1 event was estimated. However, it is not possible to determine which fraction of the preexisting particles were entrained from the PBL or were formed by NPF in the FT. In contrast, the contribution of PBL injections to the CCN number concentration is much higher, especially in summer (see Figure 12). The multistep growth mechanism may be important at several other high-altitude sites. To our knowledge, direct growth to CCN size has not been seen either at other high-altitude sites, e.g., at Pyramid station, Storm Peak, or Chacaltaya [*Venzac et al.*, 2008; *Rose et al.*, 2015a; *Hallar et al.*, 2011, 2016].

Possible factors controlling nucleation at the JFJ have been investigated. Meteorological factors are of minor importance, as well as the condensation sink. The condensation sink is even increased during NPF events due to the recent PBL injections, but in all cases low. Further, there are strong indications that global radiation, concentration of condensable vapors and strength of the PBL influence govern the formation rates at the JFJ, and an equation estimating the formation rate, based on these variables, or appropriate proxies, was developed (see Table 2). This nucleation parametrization could be further improved via additional long-term studies, including, for example, an additional chemical ionization APi-TOF to provide better information on the HOMs that are present during nucleation. Such work would further contribute to the improvement of FT nucleation mechanisms in large-scale models.

Acknowledgments

We thank the International Foundation High Altitude Research Stations Jungfraujoch and Gornergrat (HFSJG) for the opportunity to perform experiments on the Jungfraujoch. In particular, we would like to thank the research station's custodians Joan and Martin Fischer and Maria and Urs Otz for their support and hospitality. The Swiss National Air Pollution Monitoring Network is run by Empa in collaboration with the Swiss Federal Office for the Environment. This work was supported by MeteoSwiss in the framework of the Global Atmosphere Watch program, FP7 project ACTRIS (grant agreement 262254) and FP7 project BACCHUS (grant agreement 603445) and the Swiss National Science Foundation, SNSF grants 200021_140663 and 200020_152907. J.T. was supported by the EC Seventh Framework Programme (Marie Curie Initial Training Network "CLOUDTRAIN") (316662). M.G. was supported by the ERC (ERC-CoG 615922-BLACARAT). The SMPS data used in this work have been submitted to EBAS and will be available for download at http://ebas.nilu.no. Trace gas data are submitted annually to http://ds.data.jma.go.jp/gmd/wdcgg/. Meteorological data are available from MeteoSwiss. All data and results can be requested from the corresponding author at martin.gysel@psi.ch or j.troestl@gmx.net.

References

Betha, R., D. V. Spracklen, and R. Balasubramanian (2013), Observations of new aerosol particle formation in a tropical urban atmosphere, *Atmos. Environ.*, *71*, 340–351, doi:10.1016/j.atmosenv.2013.01.049.

Bianchi, F., et al. (2016), New particle formation in the free troposphere: A matter of chemistry and timing, *Science*, *352*(6289), 1109–1112, doi:10.1126/science.aad5456.

Boulon, J., et al. (2010), New particle formation and ultrafine charged aerosol climatology at a high altitude site in the Alps (Jungfraujoch, 3580 m asl, Switzerland), *Atmos. Chem. Phys.*, *10*(19), 9333–9349, doi:10.5194/acp-10-9333-2010.

Boulon, J., K. Sellegri, M. Hervo, D. Picard, J.-M. Pichon, P. Fréville, and P. Laj (2011), Investigation of nucleation events vertical extent: A long term study at two different altitude sites, *Atmos. Chem. Phys.*, *11*(12), 5625–5639, doi:10.5194/acp-11-5625-2011.

Bukowiecki, N., E. Weingartner, M. Gysel, M. Collaud Coen, P. Zieger, E. Herrmann, M. Steinbacher, H. W. Gäggeler, and U. Baltensperger (2016), A review of more than 20 years of aerosol observation at the high altitude research station Jungfraujoch, Switzerland (3580 m asl), *Aerosol Air Qual. Res.*, *16*(3), 764–788, doi:10.4209/aaqr.2015.05.0305.

Carslaw, K. S., et al. (2013), Large contribution of natural aerosols to uncertainty in indirect forcing, *Nature*, *503*(7474), 67–71, doi:10.1038/nature12674.

Collaud Coen, M., E. Weingartner, M. Furger, S. Nyeki, A. S. H. Prévôt, M. Steinbacher, and U. Baltensperger (2011), Aerosol climatology and planetary boundary influence at the Jungfraujoch analyzed by synoptic weather types, *Atmos. Chem. Phys.*, *11*(12), 5931–5944, doi:10.5194/acp-11-5931-2011.

Fröhlich, R., et al. (2015), Fourteen months of on-line measurements of the non-refractory submicron aerosol at the Jungfraujoch (3580 m a.s.l.)—Chemical composition, origins and organic aerosol sources, *Atmos. Chem. Phys.*, *15*(19), 11,373–11,398, doi:10.5194/acp-15-11373-2015.

García, M. I., S. Rodríguez, Y. González, and R. D. García (2014), Climatology of new particle formation at Izaña mountain GAW observatory in the subtropical North Atlantic, *Atmos. Chem. Phys.*, *14*(8), 3865–3881, doi:10.5194/acp-14-3865-2014.

Hallar, A. G., D. H. Lowenthal, G. Chirokova, R. D. Borys, and C. Wiedinmyer (2011), Persistent daily new particle formation at a mountain-top location, *Atmos. Environ.*, *45*(24), 4111–4115, doi:10.1016/j.atmosenv.2011.04.044.

Hallar, A. G., R. Petersen, I. B. McCubbin, D. Lowenthal, S. Lee, E. Andrews, and F. Yu (2016), Climatology of new particle formation and corresponding precursors at Storm Peak Laboratory, *Aerosol Air Qual. Res.*, *16*, 816–826, doi:10.4209/aaqr.2015.05.0341.

Hammer, E., N. Bukowiecki, M. Gysel, Z. Jurányi, C. R. Hoyle, R. Vogt, U. Baltensperger, and E. Weingartner (2014), Investigation of the effective peak supersaturation for liquid-phase clouds at the high-alpine site Jungfraujoch, Switzerland (3580 m asl), *Atmos. Chem. Phys.*, *14*(2), 1123–1139, doi:10.5194/acp-14-1123-2014.

Henne, S., M. Furger, and A. S. H. Prévôt (2005a), Climatology of mountain venting-induced elevated moisture layers in the lee of the Alps, *J. Appl. Meteorol.*, *44*(5), 620–633, doi:10.1175/JAM2217.1.

Henne, S., J. Dommen, B. Neininger, S. Reimann, J. Staehelin, and A. S. H. Prévôt (2005b), Influence of mountain venting in the Alps on the ozone chemistry of the lower free troposphere and the European pollution export, *J. Geophys. Res.*, *110*, D22307, doi:10.1029/2005JD005936.

Herrmann, E., et al. (2015), Analysis of long-term aerosol size distribution data from Jungfraujoch with emphasis on free tropospheric conditions, cloud influence, and air mass transport, *J. Geophys. Res. Atmos.*, *120*, 9459–9480, doi:10.1002/2015JD023660.

Hirsikko, A., T. Bergman, L. Laakso, M. Dal Maso, I. Riipinen, U. Hõrrak, and M. Kulmala (2007), Identification and classification of the formation of intermediate ions measured in boreal forest, *Atmos. Chem. Phys.*, *7*(1), 201–210, doi:10.5194/acp-7-201-2007.

Järvinen, E., et al. (2013), Seasonal cycle and modal structure of particle number size distribution at Dome C, Antarctica, *Atmos. Chem. Phys.*, *13*, 7473–7487, doi:10.5194/acp-13-7473-2013.

Jurányi, Z., M. Gysel, E. Weingartner, N. Bukowiecki, L. Kammermann, and U. Baltensperger (2011), A 17 month climatology of the cloud condensation nuclei number concentration at the high alpine site Jungfraujoch, *J. Geophys. Res.*, *116*, D10204, doi:10.1029/2010JD015199.

Kirkby, J., et al. (2011), Role of sulphuric acid, ammonia and galactic cosmic rays in atmospheric aerosol nucleation, *Nature*, *476*(7361), 429–433, doi:10.1038/nature10343.

Kirkby, J., et al. (2016), Ion-induced nucleation of pure biogenic particles, *Nature*, *533*(7604), 521–526, doi:10.1038/nature17953.

Kulkarni, P., P. A. Baron, and K. Willeke (2011), *Aerosol Measurement: Principles, Techniques, and Applications*, John Wiley, Hoboken, N. J.

Kulmala, M., et al. (2012), Measurement of the nucleation of atmospheric aerosol particles, *Nat. Protoc.*, *7*(9), 1651–1667, doi:10.1038/nprot.2012.091.

Kulmala, M., et al. (2013), Direct observations of atmospheric aerosol nucleation, *Science*, *339*(6122), 943–946, doi:10.1126/science.1227385.

Kulmala, M., T. Petäjä, M. Ehn, J. Thornton, M. Sipilä, D. R. Worsnop, and V.-M. Kerminen (2014), Chemistry of atmospheric nucleation: On the recent advances on precursor characterization and atmospheric cluster composition in connection with atmospheric new particle formation, *Annu. Rev. Phys. Chem.*, *65*, 21–37, doi:10.1146/annurev-physchem-040412-110014.

Kürten, A., C. Williamson, J. Almeida, J. Kirkby, and J. Curtius (2015), On the derivation of particle nucleation rates from experimental formation rates, *Atmos. Chem. Phys.*, *15*(8), 4063–4075, doi:10.5194/acp-15-4063-2015.

Liu, S., M. Hu, Z. Wu, B. Wehner, A. Wiedensohler, and Y. Cheng (2008), Aerosol number size distribution and new particle formation at a rural/coastal site in Pearl River Delta (PRD) of China, *Atmos. Environ.*, *42*(25), 6275–6283, doi:10.1016/j.atmosenv.2008.01.063.

Merikanto, J., D. V. Spracklen, G. W. Mann, S. J. Pickering, and K. S. Carslaw (2009), Impact of nucleation on global CCN, *Atmos. Chem. Phys.*, *9*(21), 8601–8616, doi:10.5194/acp-9-8601-2009.

Neitola, K., E. Asmi, M. Komppula, A.-P. Hyvärinen, T. Raatikainen, T. S. Panwar, V. P. Sharma, and H. Lihavainen (2011), New particle formation infrequently observed in Himalayan foothills—Why?, *Atmos. Chem. Phys.*, *11*(16), 8447–8458, doi:10.5194/acp-11-8447-2011.

Nyeki, S., U. Baltensperger, I. Colbeck, D. T. Jost, E. Weingartner, and H. W. Gäggeler (1998), The Jungfraujoch high-alpine research station (3454 m) as a background clean continental site for the measurement of aerosol parameters, *J. Geophys. Res.*, *103*(D6), 6097–6107, doi:10.1029/97JD03123.

Nyeki, S., et al. (2000), Convective boundary layer evolution to 4 km asl over high-alpine terrain: Airborne lidar observations in the Alps, *Geophys. Res. Lett.*, *27*(5), 689–692, doi:10.1029/1999GL010928.

Nyeki, S., K. Eleftheriadis, U. Baltensperger, I. Colbeck, M. Fiebig, A. Fix, C. Kiemle, M. Lazaridis, and A. Petzold (2002), Airborne lidar and in-situ aerosol observations of an elevated layer, leeward of the European Alps and Apennines, *Geophys. Res. Lett.*, *29*(17), 1852, doi:10.1029/2002GL014897.

O'Dowd, C., C. Monahan, and M. Dall'Osto (2010), On the occurrence of open ocean particle production and growth events, *Geophys. Res. Lett.*, *37*, L19805, doi:10.1029/2010GL044679.

Pandey Deolal, S., D. Brunner, M. Steinbacher, U. Weers, and J. Staehelin (2012), Long-term in situ measurements of NO_x and NO_y at Jungfraujoch 1998–2009: Time series analysis and evaluation, *Atmos. Chem. Phys.*, *12*(5), 2551–2566, doi:10.5194/acp-12-2551-2012.

Rose, C., et al. (2015a), Frequent nucleation events at the high altitude station of Chacaltaya (5240 m asl), Bolivia, *Atmos, Environ,102*, 18–29, doi:10.1016/j.atmosenv.2014.11.015.

Rose, C., K. Sellegri, E. Freney, R. Dupuy, A. Colomb, J.-M. Pichon, M. Ribeiro, T. Bourianne, F. Burnet, and A. Schwarzenboeck (2015b), Airborne measurements of new particle formation in the free troposphere above the Mediterranean Sea during the HYMEX campaign, *Atmos. Chem. Phys.*, *15*(17), 10,203–10,218, doi:10.5194/acp-15-10203-2015.

Seinfeld, J. H., and S. N. Pandis (2006), *Atmospheric Chemistry and Physics: From Air Pollution to Climate Change*, John Wiley, Hoboken, N. J.

Stohl, A., C. Forster, A. Frank, P. Seibert, and G. Wotawa (2005), Technical note: The Lagrangian particle dispersion model FLEXPART version 6.2, *Atmos. Chem. Phys.*, *5*(9), 2461–2474, doi:10.5194/acp-5-2461-2005.

Tröstl, J., et al. (2016), The role of low-volatility organic compounds in initial particle growth in the atmosphere, *Nature*, *533*(7604), 527–531, doi:10.1038/nature18271.

Venzac, H., et al. (2008), High frequency new particle formation in the Himalayas, *Proc. Natl. Acad. Sci. U. S. A.*, *105*(41), 15,666–15,671, doi:10.1073/pnas.0801355105.

Wang, S. C., and R. C. Flagan (1990), Scanning electrical mobility spectrometer, *Aerosol Sci. Technol.*, *13*(2), 230–240, doi:10.1080/02786829008959441.

Weingartner, E., S. Nyeki, and U. Baltensperger (1999), Seasonal and diurnal variation of aerosol size distributions ($10 < d < 750$ nm) at a high-alpine site (Jungfraujoch 3580 m asl), *J. Geophys. Res.*, *104*(D21), 26,809–26,820, doi:10.1029/1999JD900170.

Wiedensohler, A., et al. (2012), Mobility particle size spectrometers: Harmonization of technical standards and data structure to facilitate high quality long-term observations of atmospheric particle number size distributions, *Atmos. Meas. Tech.*, *5*, 657–685, doi:10.5194/amt-5-657-2012.

Wimmer, D., et al. (2015), Technical note: Using DEG-CPCs at upper tropospheric temperatures, *Atmos. Chem. Phys.*, *15*(13), 7547–7555, doi:10.5194/acp-15-7547-2015.

Xiao, S., et al. (2015), Strong atmospheric new particle formation in winter in urban Shanghai, China, *Atmos. Chem. Phys.*, *15*(4), 1769–1781, doi:10.5194/acp-15-1769-2015.

Yli-Juuti, T., et al. (2011), Growth rates of nucleation mode particles in Hyytiälä during 2003–2009: Variation with particle size, season, data analysis method and ambient conditions, *Atmos. Chem. Phys.*, *11*(24), 12,865–12,886, doi:10.5194/acp-11-12865-2011.

Yu, F., and A. G. Hallar (2014), Difference in particle formation at a mountaintop location during spring and summer: Implications for the role of sulfuric acid and organics in nucleation, *J. Geophys. Res. Atmos.*, *119*, 12,246–12,255, doi:10.1002/2014JD022136.

Zellweger, C., J. Forrer, P. Hofer, S. Nyeki, B. Schwarzenbach, E. Weingartner, M. Ammann, and U. Baltensperger (2003), Partitioning of reactive nitrogen (NO_y) and dependence on meteorological conditions in the lower free troposphere, *Atmos. Chem. Phys.*, *3*(3), 779–796, doi:10.5194/acp-3-779-2003.

Zellweger, C., M. Steinbacher, and B. Buchmann (2012), Evaluation of new laser spectrometer techniques for in-situ carbon monoxide measurements, *Atmos. Meas. Tech.*, *5*(10), 2555–2567, doi:10.5194/amt-5-2555-2012.